ChemComm

COMMUNICATION

View Article Online
View Journal | View Issue

Cite this: *Chem. Commun.*, 2019, 55, 5283

Received 20th February 2019,
Accepted 9th April 2019

DOI: 10.1039/c9cc01446b

rsc.li/chemcomm

A multifunctional persistent luminescent nanoprobe for imaging guided dual-stimulus responsive and triple-synergistic therapy of drug resistant tumor cells†

Feng-Xia Su, [b] Xu Zhao, [ac] Cong Dai, [d] Yu-Jie Li, [d] Cheng-Xiong Yang [d] and Xiu-Ping Yan *[ac]

We report the design and fabrication of a multifunctional persistent luminescent nanoprobe for imaging guided dual-stimulus responsive and triple-synergistic therapy of drug resistant tumor. The integration of the dual-stimulus of an acidic microenvironment and laser irradiation with the triple-synergistic therapy of doxorubicin, photothermal and siRNA offers excellent therapeutic performance for drug resistant tumor cells with high specificity and little side effects.

The long-term use of chemotherapeutic drugs in cancer treatment can easily lead to multiple drug resistance (MDR) of tumor, which decreases chemotherapeutic efficiency.[1–3] MDR mainly results from the overexpressed drug efflux transporters on the cytomembrane, such as P-glycoprotein (P-gp), which is capable of transporting chemotherapeutic drugs out of cells to decrease cytotoxicity.[4,5] Small interfering RNA (siRNA) is able to down-regulate the expression of MDR1 mRNA and P-gp to elevate chemotherapeutic efficiency.[6–8] Then, various strategies for co-delivering siRNA and anticancer drugs on a single nanocarrier have been demonstrated to be more effective than each individual monotherapy.[9–12] Nevertheless, the tumor non-specificity of the existing nanomedicines is the main cause of toxicity to normal cells.

Tumor specific ligands can increase the accumulation of therapeutic agents at tumor sites and reduce the side effects of anticancer drugs, showing more clinical significance.[13,14] At the same time, the safety issue resulting from off-target effects indicates that nanomedicines need more selective therapeutic conditions. Smart nanosystems based on stimulus-responsive therapy have received increasing attention due to the gained targeting therapeutic specificity of the nanomedicine. For example, the abnormal acidic microenvironment of tumor enables the low pH responsive release of drug and siRNA.[15,16]

The therapeutic efficacy of siRNA assisted chemotherapy mainly relies on the P-gp silencing efficiency of siRNA. Off-target effects of siRNA may potentially lead to low therapeutic performance.[17] Photothermal therapy has attracted much attention due to it being less invasive than traditional tumor destruction methods[18,19] and its enhancing effect on tumor susceptibility to chemotherapy.[20,21] So, photothermal therapy is a good candidate to overcome drug resistance to increase the efficacy of thermotherapy and reduce side effects. Heat is induced by an external local stimulus after the nanomedicine has targeted tumor cells. Therefore, precise imaging guidance to monitor the direction of the nanomedicine and the tumor location is urgently needed.

Persistent luminescent nanoparticles (PLNPs) possess good biocompatibility and long-lasting afterglow, allowing autofluorescence free bioimaging without the need for *in situ* excitation.[22–26] Persistent luminescence of near-infrared (NIR) PLNPs can be activated with red photons that possess high penetration and low energy. Thus, NIR emitting PLNP based probes are attractive for imaging guided nanomedicine delivery and guided therapy.

Herein, we report the design and fabrication of a multifunctional persistent luminescent nanoprobe for imaging-guided dual-stimulus responsive and triple-synergistic therapy of MDR tumor cells (Fig. 1a). Monodispersed hydroxyl functionalized $Zn_{1.1}Ga_{1.8}Ge_{0.1}O_4$:0.5%$Cr^{3+}$,0.5%$Eu^{3+}$ PLNP (PLNP-OH) is used as the core due to its reactivatable NIR persistent luminescence by 650 nm LED light,[27] while poly dopamine (PDA) is employed as the shell to produce heat under laser irradiation and load doxorubicin (DOX) though π–π stacking.[28,29] Further conjugation with folic acid (FA) modified polyethyleneimine (PEI-FA) improves the biocompatibility and provides the ability of active tumor-targeting and siRNA loading.[30] The acidic microenvironment promotes the release of siRNA from PEI *via* a "proton sponge" effect.[31] Meanwhile, the acidic microenvironment facilitates the

[a] *State Key Laboratory of Food Science and Technology, Jiangnan University, Wuxi 214122, China. E-mail: xpyan@jiangnan.edu.cn*
[b] *School of Chemistry and Biological Engineering, University of Science and Technology Beijing, 30 Xueyuan Road, Beijing 100083, China*
[c] *International Joint Laboratory on Food Safety, Institute of Analytical Food Safety, School of Food Science and Technology, Jiangnan University, Wuxi 214122, China*
[d] *Research Center for Analytical Science, Tianjin Key Laboratory of Molecular Recognition and Biosensing, College of Chemistry, Nankai University, Tianjin 300071, China*

† Electronic supplementary information (ESI) available: Experimental details and additional figures. See DOI: 10.1039/c9cc01446b

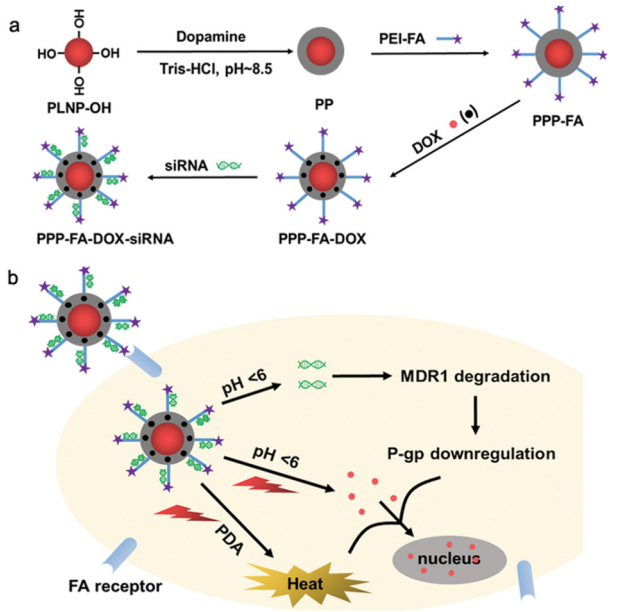

Fig. 1 (a) Scheme for the synthesis of the multifunctional persistent luminescent nanoprobe (PPP-FA-DOX-siRNA). (b) Illustration of the multifunctional persistent luminescent nanoprobe for imaging guided dual-stimulus responsive and triple-synergistic therapy of MDR tumor cells.

protonation of the daunosamine group and diminishes the hydrophobic π–π stacking interaction,[32] thus triggering DOX release. Laser irradiation triggers PDA to produce heat and facilitates DOX release (Fig. 1b). This multifunctional nanoprobe integrates the dual-stimulus of the acidic microenvironment and laser irradiation with the triple-synergistic therapy of DOX, photothermal and siRNA, enabling excellent therapeutic performance on drug resistant tumor cells with high specificity and little side effects.

PLNP-OH was prepared according to our previous work[27] with slight modifications (ESI†). PDA was coated on PLNP-OH *via* self-polymerization of dopamine. PEI-FA was prepared from PEI and FA through an acylation reaction (Fig. S1a and b, ESI†). The PDA-coated PLNP (PP) was further functionalized with PEI-FA *via* Schiff base reaction between the oxidized quinone of catechol and the amines of PEI-FA. Finally, DOX and siRNA were adsorbed on the PEI-FA functionalized PP (PPP-FA) through π–π stacking and electrostatic interactions to get the multifunctional nanoprobe PLNP-PDA-PEI-FA-DOX-siRNA (PPP-FA-DOX-siRNA).

The core PLNP-OH has a pure spinel phase structure of $ZnGa_2O_4$ and Zn_2GeO_4 (Fig. S2b, ESI†) with an average diameter of 35.4 nm (Fig. S2a, ESI†). Coating of PDA on PLNP-OH changed the zeta potential from −18.3 mV to −29.7 mV due to the –OH groups on the PDA shells (Fig. S3, ESI†). The PDA shell exhibited a thickness of 3.33 nm (Fig. S4c, ESI†). The characteristic peaks at 284 nm and 370 nm in the UV-Vis absorption spectrum (Fig. S5a, ESI†) and the band of the –CONH– stretching vibration at 1660 cm^{-1} in FT-IR spectrum (Fig. S5b, ESI†) confirm the successful conjugation of PEI-FA and PP. Besides, the change in zeta potential from negative (−29.7 mV) to positive (+35.8 mV) also confirms the successful functionalization of PEI-FA on PP

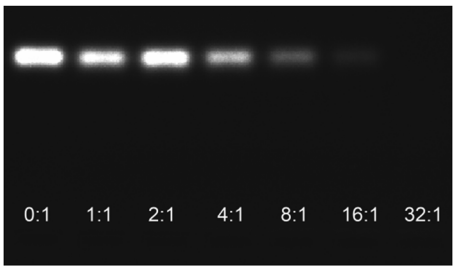

Fig. 2 Agarose gel electrophoretic assay of PPP-FA-DOX-(P-gp) siRNA at various weight ratios (PPP-FA-DOX : P-gp siRNA): 0 : 1, 1 : 1, 2 : 1, 4 : 1, 8 : 1, 16 : 1, and 32 : 1.

(Fig. S3, ESI†). The new peak in the UV-Vis absorption and fluorescence spectra (Fig. S5a and S6, ESI†) along with the slight change of zeta potential (Fig. S3, ESI†) suggest the successful loading of DOX. The extent of DOX loaded on PPP-FA was 254 μg mg^{-1}.

P-gp siRNA binds to PPP-FA-DOX through electrostatic interaction, forming PPP-FA-DOX-(P-gp) siRNA. The binding capacity was investigated by using agarose gel electrophoresis. The brightness of the free P-gp siRNA band decreased as the weight ratio (w/w) of PPP-FA-DOX/P-gp siRNA increased, indicating that the binding efficiency of P-gp siRNA increased with the weight ratio (Fig. 2). P-gp siRNA was completely absorbed on PPP-FA-DOX at the weight ratio of 32 : 1, and the extent of P-gp siRNA loaded on PPP-FA-DOX was 31.25 μg mg^{-1}.

The as-prepared PLNP-OH core gave a NIR phosphorescence emission peak at 695 nm with a long lasting NIR luminescence afterglow under 254 nm UV light excitation (Fig. 3a and Fig. S7a, b, S8a, ESI†). Moreover, the phosphorescence and NIR luminescence afterglow of PLNP-OH can be reactivated by a red LED light (Fig. S8b, ESI†), providing great potential for long-term autofluorescence free *in vivo* imaging.

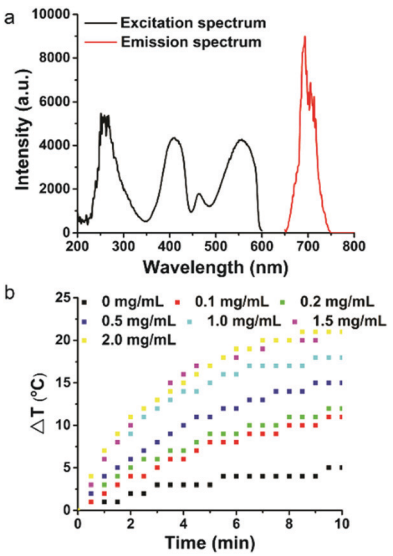

Fig. 3 (a) Excitation and emission spectra of the as-prepared PLNP-OH powder. (b) Temperature change of PP at various concentrations under 808 nm laser irradiation (2 W cm^{-2}, 10 min).

We first optimized the amount of dopamine as the NIR absorption capacity of PDA has an impact on PLNP luminescence and photothermal conversion ability. The temperature increment of PP increased with the amount of dopamine (Fig. S4b, ESI†), whereas the luminescence intensity of PP decreased, which is unfavourable for bioimaging (Fig. S4a and S9, ESI†). Considering both the photothermal conversion efficiency and the luminescence intensity, 70 μg of dopamine was chosen as a compromise to react with 1 mg of PLNP-OH to get PP.

We then investigated the temperature change of PP at different concentrations under 808 nm laser irradiation (2 W cm^{-2}) for 10 min (Fig. 3b). These results show that the prepared PP exhibits a distinct increase of temperature upon 808 nm laser irradiation and displayed a time- and concentration-dependent trend. The temperature of different concentrations of PP solution rose from the initial 25 °C to a different maximum temperature from 37 °C to 45 °C.

DOX release was examined in aqueous solutions at pH 5.5 and pH 7.4 to simulate the tumor acidic microenvironment and normal physiological environment, respectively. The solutions were treated with or without 808 nm laser irradiation for 10 min at a fixed time interval. 54.0% and 21.1% DOX were released at pH 5.5 and pH 7.4, respectively, after incubation for 48 h and irradiation at a fixed time interval. In contrast, 46.3% and 17.0% DOX were released at pH 5.5 and pH 7.4, respectively, without irradiation (Fig. 4). These results demonstrate that the acidic environment made DOX more water soluble and easy to release while the laser irradiation also accelerated DOX release. The sustained site-specific release process of DOX may potentially avoid side effects in further *in vivo* applications.

The above results encouraged us to apply the multifunctional PLNP nanoprobe in cell imaging and therapy. Both 293T cells (normal cells, FA receptor low-expressed) and MCF-7/ADR cells (DOX resistant MCF-7 cells, FA receptor over-expressed) were employed as model cells. The confocal laser scanning microscopy (CLSM) images (Fig. 5) show that more PPP-FA was internalized in the MCF-7/ADR cells than 293T cells. To better verify the selectivity of the nanoprobe, MCF-7/ADR cells whose FA receptor was blocked with FA were subsequently incubated with PPP-FA. The results show that the amount of nanoprobe entering the untreated cells was higher than that entering the blocked cells (Fig. S10, ESI†), suggesting that PPP-FA offered the ability of targeting and imaging tumor cells.

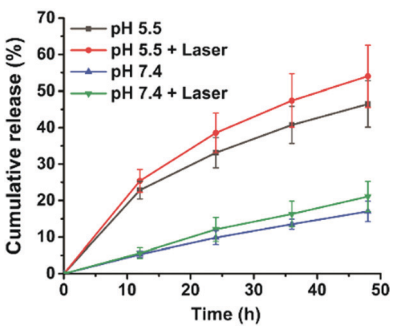

Fig. 4 DOX release profile at pH 5.5 and 7.4, treated with or without 808 nm laser irradiation (2 W cm^{-2}, 10 min) over 48 h.

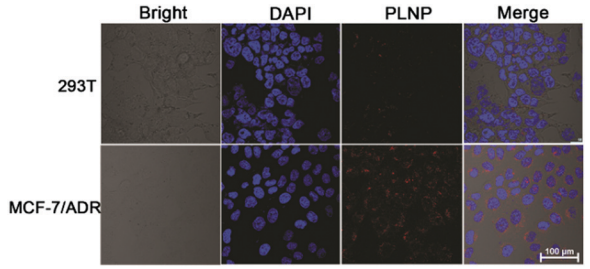

Fig. 5 CLSM images of 293T and MCF-7/ADR cells after incubation with PPP-FA. Scale bar = 100 μm.

The light assisted DOX release behavior of the nanoprobe was evaluated using MCF-7/ADR cells. The drug resistance of MCF-7/ADR cells compared with MCF-7 cells was firstly tested by incubating with free DOX. Strong fluorescence of DOX was observed in the nucleus of the MCF-7 cells (Fig. S11, ESI†), whereas little free DOX entered the MCF-7/ADR cells, indicating the drug efflux property of the MCF-7/ADR cells. MCF-7/ADR cells were also incubated with PPP-FA-DOX under 808 nm laser irradiation or not (2 W cm^{-2}, 10 min). Incubation of MCF-7/ADR cells with PPP-FA-DOX gave stronger DOX fluorescence than that with free DOX because the nanoprobe entered the cells in a FA-mediated manner. Due to the sustained release process and drug efflux, most DOX remained in the cytoplasm at the time of our observation. However, when the nanoprobes entering the cells were exposed to laser irradiation, the released amount of DOX increased, and the amount of DOX entering the nucleus also increased (Fig. S11, ESI†), thereby increasing the sensitivity of the MCF-7/ADR cells to DOX, which may be the key factor contributing to the synergistic therapy effect of DOX and photothermal on drug-resistant tumor cells.

MCF-7/ADR cells were also incubated with free P-gp siRNA and PPP-FA-(P-gp) siRNA, which results from electrostatic binding of PPP-FA and P-gp siRNA. P-gp siRNA was labelled with 6-carboxyfluorescein (FAM) to verify the delivery ability of the nanoprobe for siRNA. The FAM fluorescence in MCF-7/ADR cells incubated with PPP-FA-(P-gp) siRNA was clearly stronger than that with free P-gp siRNA (Fig. S12, ESI†), indicating that the free P-gp siRNA scarcely entered the MCF-7/ADR cells, but P-gp siRNA on the nanoprobe could enter the MCF-7/ADR cells through endocytosis.

Efficient knockdown of a drug resistant gene can elevate the internalized amounts of drugs and chemotherapeutic effect in drug resistant tumor cells. So, the knockdown efficiency of MDR1 mRNA and P-gp expression was assayed. The quantitative reverse transcription-PCR results indicate that PPP-FA-(P-gp) siRNA gave a higher MDR1 mRNA knockdown efficiency (43%) than other control groups (Fig. S13a, ESI†). PPP-FA-(P-gp) siRNA also had a higher P-gp silencing efficiency (41%) compared with other control groups (Fig. S13b, ESI†).

MTT assays were performed to evaluate the potential anti-tumor activity of the multifunctional nanoprobe. The viability of MCF-7/ADR cells incubated with different nanoprobes displayed a concentration-dependent manner (Fig. S14, ESI†). PPP-FA-DOX and DOX gave similar cytotoxicity, likely due to the sustained release

of DOX from the nanoprobe. 120 μg mL^{-1} PPP-FA-DOX-(P-gp) siRNA showed a cell viability decrease of about 20% compared with PPP-FA-DOX, indicating that P-gp siRNA downregulated the expression level of P-gp and elevated the chemotherapy efficiency. The photothermal effect caused the viability of cells incubated with 120 μg mL^{-1} PPP-FA-DOX-(P-gp) siRNA to further decrease to 27%. The triple synergistic cell killing effect was higher than the sum of PPP-FA-DOX-(P-gp) siRNA (67% alive) and the photothermal effect (68% alive), indicating that the photothermal effect accelerated the release of DOX and improve the efficiency of entering the nucleus. PPP-FA-DOX under laser gave a higher cell killing effect of 58% cells death compared to the sum of PPP-FA-DOX (13% death) and the photothermal effect (32% death), while laser irradiation itself showed no cytotoxicity on MCF-7/ADR cells (Fig. S15, ESI†). The results demonstrate that the multifunctional nanoprobe not only co-delivered anticancer drugs, but also produced a triple-synergistic therapeutic effect for drug resistant tumor cells.

To show the potential application ability of the nanoprobe *in vivo*, the preliminary imaging effect was tested in MCF-7 cell tumor-bearing mice. The nanoprobe was pre-irradiated with UV light for 10 minutes and subsequently intratumorally injected into the mice. The mice were irradiated with red LED light for 5 minutes before acquiring luminescence images each time. The tumor still had obvious luminescence 4 h after injection (Fig. S16, ESI†), which proves the stability of the long afterglow luminescence. More importantly, since the luminescence images were collected without *in situ* excitation, no interference of background bioluminescence was observed, while the fluorescence of DOX under 500 nm excitation had strong background interference (Fig. S17, ESI†).

In conclusion, we have reported a multifunctional persistent luminescent nanoprobe for imaging guided dual-stimulus responsive and triple-synergistic therapy for drug resistant tumor cells. The FA and the persistent luminescence of the nanoprobe provided precise autofluorescence-free optical imaging guidance for therapy. The dual-stimulus of 808 nm laser irradiation and the acidic microenvironment triggered siRNA and DOX release while 808 nm laser irradiation stimulates the nanoprobe to produce heat and accelerates DOX release, avoiding non-specific targeting and side effects. DOX, siRNA and photothermal exhibit good triple-synergistic therapeutic performance towards MDR tumor cells, showing great potential in MDR tumor applications. In future, the multifunctional nanoprobe will be further explored in the treatment of drug resistant tumor *in vivo*.

This work was supported by the National Natural Science Foundation of China (No. 21435001), the National First-class Discipline Program of Food Science and Technology (No. JUFSTR20180301), and the Fundamental Research Funds for the Central Universities (No. JUSRP51714B).

Conflicts of interest

There are no conflicts of interest to declare.

Notes and references

1 S. A. Eccles, E. O. Aboagye and S. Ali, *Breast Cancer Res.*, 2013, **15**, R92.
2 A. Palmeira, E. Sousa, M. H. Vasconcelos and M. M. Pinto, *Curr. Med. Chem.*, 2012, **19**, 1946.
3 M. P. V. Shekhar, *Curr. Cancer Drug Targets*, 2011, **11**, 613.
4 S. G. Aller, J. Yu, A. Ward, Y. Weng, S. Chittaboina, R. P. Zhuo, P. M. Harrell, Y. T. Trinh, Q. H. Zhang and I. L. Urbatsch, *Science*, 2009, **323**, 1718.
5 P. D. W. Eckford and F. J. Sharom, *Chem. Rev.*, 2009, **109**, 2989.
6 H. Wu, W. N. Hait and J. M. Yang, *Cancer Res.*, 2003, **63**, 1515.
7 E. B. Logashenko, A. V. Vladimirova, M. N. Repkova, A. G. Venyaminova, E. L. Chernolovskaya and V. V. Vlassov, *Nucleosides, Nucleotides Nucleic Acids*, 2004, **23**, 861.
8 J. M. Li, Y. Y. Wang, M. X. Zhao, C. P. Tan, Y. Q. Li, X. Y. Le, L. N. Ji and Z. W. Mao, *Biomaterials*, 2012, **33**, 2780.
9 H. Meng, M. Liong, T. Xia, Z. Li, Z. Ji, J. I. Zink and A. E. Nel, *ACS Nano*, 2010, **4**, 4539.
10 M. Saad, O. B. Garbuzenko and T. Minko, *Nanomedicine*, 2008, **3**, 761.
11 C. He, C. Poon, C. Chan, S. D. Yamada and W. Lin, *J. Am. Chem. Soc.*, 2016, **138**, 6010.
12 M. Wu, Q. Meng, Y. Chen, L. Zhang, M. Li, X. Cai, Y. Li, P. Yu, L. Zhang and J. Shi, *Adv. Mater.*, 2016, **28**, 1963.
13 T. L. Kaneshiro and Z.-R. Lu, *Biomaterials*, 2009, **30**, 5660.
14 X.-B. Xiong and A. Lavasanifar, *ACS Nano*, 2011, **5**, 5202.
15 G.-F. Luo, X.-D. Xu, J. Zhang, J. Yang, Y.-H. Gong, Q. Lei, H.-Z. Jia and C. Li, *ACS Appl. Mater. Interfaces*, 2012, **4**, 5317.
16 W.-Q. Li, Z. Wang, S. Hao, H. He, Y. Wan, C. Zhu, L.-P. Sun, G. Cheng and S.-Y. Zheng, *ACS Appl. Mater. Interfaces*, 2017, **9**, 16793.
17 J. Zhao and S.-S. Feng, *Nanomedicine*, 2015, **10**, 2199.
18 R. W. Habash, R. Bansal, D. Krewski and H. T. Alhafid, *Crit. Rev. Biomed. Eng.*, 2006, **34**, 491.
19 R. W. Habash, R. Bansal, D. Krewski and H. T. Alhafid, *Crit. Rev. Biomed. Eng.*, 2006, **34**, 459.
20 D. Jaque, L. M. Maestro, B. del Rosal, P. Haro-Gonzalez, A. Benayas, J. L. Plaza, E. M. Rodrígueza and J. G. Solé, *Nanoscale*, 2014, **6**, 9494.
21 B. Hildebrandt, P. Wust, O. Ahlers, A. Dieing, G. Sreenivasa, T. Kerner, R. Felix and H. Riess, *Crit. Rev. Oncol. Hemat.*, 2002, **43**, 33.
22 S.-K. Sun, H.-F. Wang and X.-P. Yan, *Acc. Chem. Res.*, 2018, **51**, 1131.
23 T. Lécuyer, E. Teston, G. Ramirez-Garcia, T. Maldiney, B. Viana, J. Seguin, N. Mignet, D. Scherman and C. Richard, *Theranostics*, 2016, **6**, 2488.
24 Q. le M. de Chermont, C. Chaneac, J. Seguin, F. Pelle, S. Maitrejean, J. P. Jolivet, D. Gourier, M. Bessodes and D. Scherman, *Proc. Natl. Acad. Sci. U. S. A.*, 2007, **104**, 9266.
25 A. Abdukayum, J.-T. Chen, Q. Zhao and X.-P. Yan, *J. Am. Chem. Soc.*, 2013, **135**, 14125.
26 T. Maldiney, A. Bessière, J. Seguin, E. Teston, S. K. Sharma, B. Viana, A. J. J. Bos, P. Dorenbos, M. Bessodes, D. Gourier, D. Scherman and C. Richard, *Nat. Mater.*, 2014, **13**, 418.
27 S.-Q. Wu, C.-W. Chi, C.-X. Yang and X.-P. Yan, *Anal. Chem.*, 2016, **88**, 4114.
28 Y. Liu, K. Ai and L. Lu, *Chem. Rev.*, 2014, **114**, 5057.
29 X. Chen, Y. Huang, G. Yang, J. Li, T. Wang, O. H. Schulz and L. K. Jennings, *Curr. Pharm. Des.*, 2015, **21**, 4262.
30 E. Wagner, *Acc. Chem. Res.*, 2011, **45**, 1005.
31 O. Boussif, F. Lezoualćh, M. A. Zanta, M. D. Mergny, D. Scherman, B. Demeneix and J. P. Behr, *Proc. Natl. Acad. Sci. U. S. A.*, 1995, **92**, 7297.
32 Y. Zeng, Z. Yang, H. Li, Y. Hao, C. Liu, L. Zhu, J. Liu, B. Lu and R. Li, *Sci. Rep.*, 2017, **7**, 43506.

